Emergence of hydrodynamic heat transport in semiconductors at the nanoscale

P. Torres,[1,*] A. Ziabari,[2,3] A. Torelló,[1] J. Bafaluy,[1] J. Camacho,[1] X. Cartoixà,[4] A. Shakouri,[2,3] and F. X. Alvarez[1]

[1]*Departament de Física, Universitat Autònoma de Barcelona, 08193 Bellaterra, Catalonia, Spain*

[2]*Birck Nanotechnology Center, Purdue University, West Lafayette, Indiana 47907, USA*

[3]*Department of Electrical and Computer Engineering, Purdue University, West Lafayette, Indiana 47907, USA*

[4]*Departament d'Enginyeria Electrònica, Universitat Autònoma de Barcelona, 08193 Bellaterra, Catalonia, Spain*

(Received 4 January 2018; published 2 July 2018)

Several recent experiments have demonstrated the failure of the Fourier heat equation in semiconductors at the nanoscale. We show that a generalized heat transport equation including a hydrodynamic term can explain three of these experiments on a silicon substrate: heater lines experiments both in stationary and nonstationary settings and the nonstationary response in grating experiments. To this end, we solve the hydrodynamic heat equation either numerically or analytically. The non-Fourier response observed in those experimental situations can be easily explained in terms of hydrodynamic concepts, such as friction and vorticity. For instance, the experimentally observed increase of thermal boundary resistance as size decreases can be simply understood as an increase of friction. We conclude that, contrary to common belief, hydrodynamics is a fundamental ingredient of semiconductor heat transport in the nanoscale at room temperature, providing physical insight and a unifying framework on the observed non-Fourier response. The relations between hydrodynamic heat transport with phonon momentum conservation and the Boltzmann transport equation are also provided.

DOI: 10.1103/PhysRevMaterials.2.076001

I. INTRODUCTION

In recent years, extensive studies of nanoscale and ultrafast heat transport have shown deviations from conventional Fourier theory [1–4]. In some experiments, Fourier's law with a thermal conductivity reduced as compared to the bulk value (effective Fourier) has been used to fit experimental data [1]. It is assumed that phonons with mean-free path larger than the system characteristic length do not contribute to the apparent thermal conductivity, thus reducing its value [4]. However, some experiments with samples including nanoscale characteristic lengths require additional suppositions to still rely on Fourier's law. This is the reason for the use of a thermal conductivity suppression function [5] in bulk materials experiments where a reduction in thermal conductivity is observed [2], and the employment of anisotropic thermal conductivity in isotropic materials like silicon in order to interpret some time domain thermoreflectance (TDTR) experiments [3].

Semiconductor heat transport at the nanoscale has some complexities due to mainly two distinct physical mechanisms. The first one is that relaxation times and mean-free paths of the different phonons can span several orders of magnitude, and consequently long jumps in the phonon random walk could give rise to abnormal diffusion described by Lévy flights [6,7]. The second issue is that, in some cases, momentum conservation in the phonon-phonon collisions can be important, introducing a hydrodynamic behavior analogous to that of fluids [8–10]. While the former has been employed to explain frequency-dependent thermal conductivity in alloys, the latter issue has received much less attention, because it is usually assumed that their effects may only be relevant at very low temperatures [11]. As a result, any structure in the flow that could come from collective or hydrodynamic effects are commonly neglected. In this article we show that heat hydrodynamic effects are ubiquitous at room temperature. We show that a generalized heat transport equation including a hydrodynamic term supplies both a unifying framework for explaining the observed non-Fourier behavior [1–4] and physical insight on the thermal response of a system depending on their time and length scales.

In the past years, some authors have shown theoretically that hydrodynamic heat transport could be important for 2D materials at room temperature [11–13]. However, the first indication of hydrodynamic heat transport at room temperature in 3D materials has only recently been demonstrated, experimentally and theoretically, through full-field thermal imaging of nanoheater lines on InGaAs semiconductor in a steady situation [14]. In this paper we show that the hydrodynamic behavior can explain the non-Fourier behavior observed not only in stationary situations but also in nonstationary experiments, and that it provides a simple interpretation of phenomena usually interpreted as a size-dependent thermal boundary resistance (TBR) or phonon suppression.

The paper is organized as follows. In Sec. II, we provide the theoretical framework underlying the hydrodynamic heat equation and its connection to the Boltzmann transport equation (BTE). In Sec. III, we solve the hydrodynamic equation, either numerically or analytically, and compare its predictions to three recent experiments displaying non-Fourier behavior on silicon. In the first experiment, we report the results of stationary temperature profiles obtained through full-field thermal imaging of nanoheater lines on top of bulk silicon; this experiment is analogous to the one previously performed

*pol.torres@uab.es

on InGaAs [14]. In the second one, we study the thermal decay of nanoheater lines on top of bulk silicon after a short heat pulse [4]. In these two cases, the complexity of the geometry does not allow an analytical solution of the hydrodynamic equation so that it is solved numerically. In the third one, we compare the thermal decay in grating experiments on silicon membranes with the analytical solution of the hydrodynamic model. In all cases a hydrodynamic interpretation of the non-Fourier response is given. Section IV is devoted to conclusions.

II. THEORETICAL FRAMEWORK

Heat or energy transport in dielectric materials, in general, can be described by the Boltzmann transport equation (BTE) for phonons. This has the form

$$\left(\frac{\partial n_{\mathbf{q}}}{\partial t}\right)_{\text{drift}} \equiv \frac{\partial n_{\mathbf{q}}}{\partial t} + \mathbf{v}_{\mathbf{q}}\frac{\partial n_{\mathbf{q}}}{\partial \mathbf{r}} = \left(\frac{\partial n_{\mathbf{q}}}{\partial t}\right)_{\text{coll}}, \tag{1}$$

where $n_{\mathbf{q}}$ is the phonon distribution function and $\mathbf{v}_{\mathbf{q}}$ is the phonon velocity. In recent years, remarkable advances have been achieved in solving the linearized Eq. (1) using first-principles calculations [15–17]. However, these approaches are limited to some simple situations. They are computationally prohibitive in a general 3D geometry because the thermal gradients appearing in the BTE are not known *a priori*.

The distribution function $n_{\mathbf{q}}$ can have an arbitrary complexity and this is one of the main problems when solving Eq. (1). However, limiting its complexity to a reduced set of its moments is usually enough to describe the temperature distribution of most experiments [9,18,19]. Our aim is to provide the simplest formalism able to capture the essential physics in Eq. (1) needed to describe the observed non-Fourier behavior. To this end, we start with the equation proposed by Guyer and Krumhansl [18–24]

$$\mathbf{Q} + \tau\frac{\partial \mathbf{Q}}{\partial t} - \ell^2(\nabla^2\mathbf{Q} + 2\nabla\nabla\cdot\mathbf{Q}) = -\kappa\boldsymbol{\nabla}T, \tag{2}$$

where $\mathbf{Q}$ is the heat flux, κ is the bulk thermal conductivity, τ is the heat flux relaxation time, and ℓ is a length parameter describing nonlocalities. The first terms on the left and the right sides of Eq. (2) define the classical Fourier's law. The second term on left-hand side describes thermal inertial effects and it is necessary when experimental time variations are of the order of the mean-free time of the phonons. In most semiconductors, this time is on the order of picoseconds, which is much smaller than the characteristic time of many pump-probe experiments, which detect temperature changes in 100s picoseconds to nanosecond range [1]. Therefore, this term will not be considered in this work. Note that this term describes second sound phenomena observed in some semiconductors at low temperatures [20]. The third term includes nonlocal effects and it depends on the nonlocal length ℓ, which is of the order of the phonon mean-free paths. This term can have two different origins. In materials where N-scattering is important, such as Si, Ge, GaAs, or diamond, this appears because of momentum conservation in normal collisions [9]. In materials where this scattering mechanism is not important like in alloys, this term is relevant when some characteristic length in the system is smaller than the phonon MFP.

Like the bulk thermal conductivity κ, both the nonlocal length ℓ and the heat flow relaxation time τ are intrinsic properties of the material, i.e., they do not depend on its geometry. The kinetic-collective model (KCM) provides explicit expressions for these quantities in terms of microscopic information such as phonon scattering rates and dispersion relations [25] which can be obtained from *ab initio* approaches. In the Supplemental Material [26] microscopic expressions for ℓ are provided, yielding typical values of the order of hundreds of nanometers for many semiconductors [8].

Interestingly, the nonlocal term in Eq. (2) is analogous to the viscous term in the Navier-Stokes equation of fluid mechanics, and it reflects the partial conservation of crystalline momentum [23]. This parallelism is the reason why Eq. (2) is usually called the phonon-hydrodynamics equation. Several works have contributed to establishing its physical grounds [20–24,27,28]. Despite the apparent simplicity of Eq. (2) with respect to Eq. (1), the possibility of solving Eq. (2) for general complex geometries through finite element methods makes it very powerful.

Notice that the nonlocal term is not necessarily in the direction of the temperature gradient and, as a result, the heat flux generated by Eq. (2) need not be parallel to the temperature gradient, a behavior that cannot be described by an effective Fourier law. This kind of phenomenon has also been recently reported in electron transport in graphene [29,30] and on heat transport in nanolayers [31]. Obviously, Eq. (2) cannot reproduce all the complexities of the phonon spectrum and interactions, such as the Lévy flights [6,7], but as we will see it can explain the main deviations from the Fourier's law observed in experiments where heat flows near a nanoscale boundary.

III. RESULTS AND DISCUSSION

Next, we compare the predictions of the hydrodynamic equation (2) to several experiments, all of them on a silicon substrate.

A. Steady state Au heater line

We first study an experiment in which a metal line is deposited on 20 nm of Al_2O_3 and about 500 μm of slightly boron doped ($\sim 1 \times 10^{16}$ cm^{-3}) silicon substrate [see Fig. 1(a)] [32]. A constant heating power is supplied to the line through an electric current and, after a while, a steady state is reached where the temperature of all the sample is constant. The amount of heat deposited in the line and the temperature rise can be independently measured using the resistance of the metal line. In addition, the temperature field on the silicon substrate can be measured through thermoreflectance thermal imaging (more details about the experimental setup and measurements are provided in Refs. [14,32]). By using heater lines of different widths, the thermal response at scales smaller than the phonon mean-free path can be observed. We have performed experiments for linewidths of 1 μm, 400 nm, and 200 nm. The results of the 400 nm experiment are displayed in Fig. 1(b). See Supplemental Material [26] for the results of the other two linewidths.

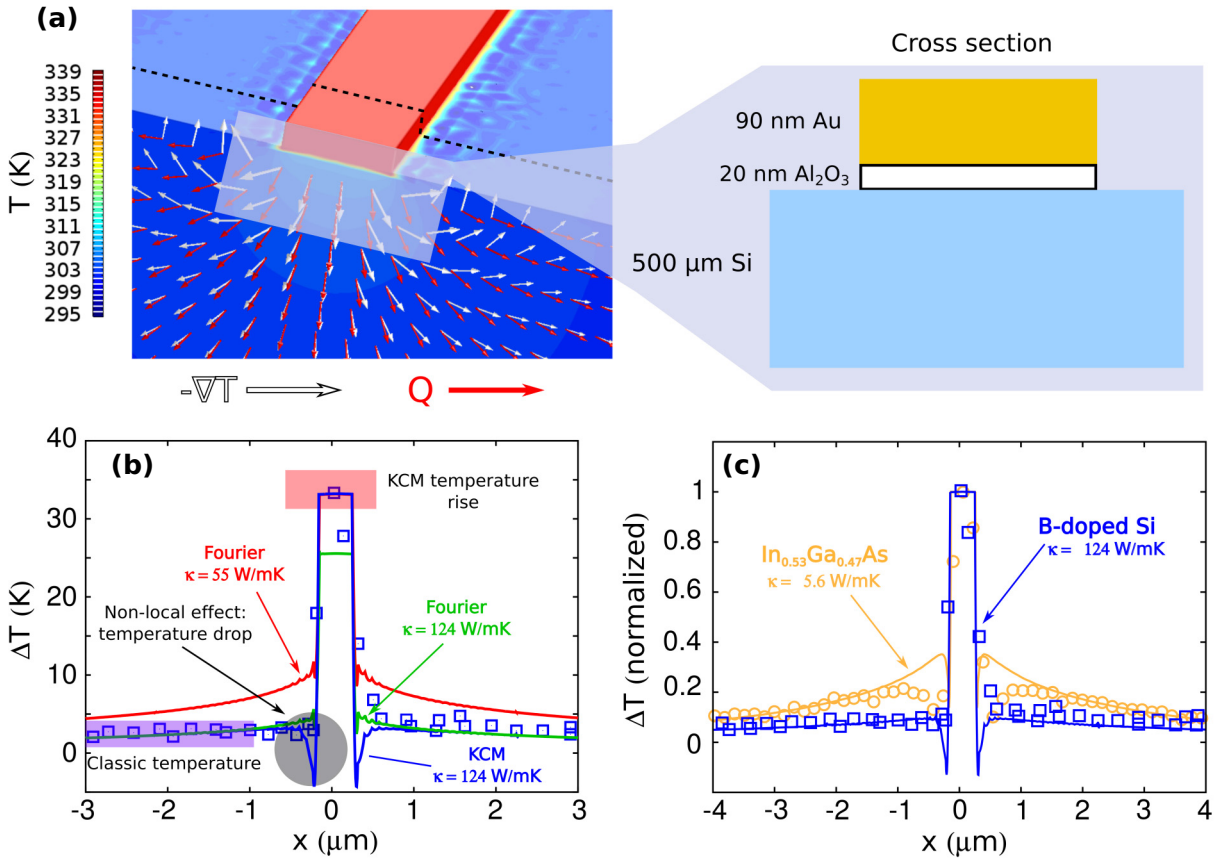

FIG. 1. (a) Calculated 3D temperature profile based on KCM (color code) and superposed heat flux vector (red arrows) with the temperature gradient (white arrows). According to the KCM model, the heat flux is not parallel to the temperature gradient due to the hydrodynamic nature of heat flowing around a corner. The dotted line represents the cross section on which the temperature profile of (b) and (c) are calculated. Details of the cross section are also provided. For more information of the experimental setup, see Refs. [14,32]. (b) Temperature cross section comparing experimental thermoreflectance thermal imaging data (symbols) with Fourier and hydrodynamic (KCM) modeling results (solid lines) of a 400 nm nanoheater line on B-doped silicon substrate with a 20 nm interlayer of Al_2O_3. (c) Comparison of the KCM results for a 400 nm heater line on top of InGaAs and B-doped Si substrate, both with a 20 nm interlayer of Al_2O_3.

Interestingly, Eq. (2) combined with the energy balance equation can be solved through finite elements using COMSOL Multiphysics [33] for this specific geometry to obtain the temperature profiles. To this end, we need to introduce the intrinsic quantities of the material, κ and ℓ, and the experimental power input. For the B-doped silicon sample the bulk experimental thermal conductivity is $\kappa = 124$ W/mK, and the nonlocal parameter $\ell = 160$ nm is obtained from microscopic quantities in Sec. S2 of the Supplemental Material (see [26]) [25].

In order to account for the interface between the Al_2O_3 oxide layer and the Si substrate, a constant TBR value of 5 nKm^2/W has been used as a free parameter to fit exactly to experimental data (see Ref. [32] and Supplemental Material [26] for more details). Let us remark that this same TBR value is used to compare theoretical predictions with the three experimental linewidths studied. In Fig. 1(b), the KCM steady state solution (blue line) for the cross section temperature profile on and around a metal line of 400 nm on top of silicon is compared with experimental data. It can be observed that KCM is able to predict the temperature profile both on the heater and the substrate surface. The sharp decay of temperature close to boundaries is a numerical artifact due to the discontinuity of the boundary; these may appear when sharp angles are used in hydrodynamic equations [34].

It is illustrative to compare the KCM solution to the predictions of an effective Fourier approach. Figure 1(b) shows that Fourier's law with a modified thermal conductivity cannot explain the full temperature distribution: by using the bulk thermal conductivity (green line), the tail of the profile can be predicted but the heater temperature is underestimated; on the other hand, if a lower effective thermal conductivity is used to reproduce the increase in the heater temperature (red line), the tail is overpredicted. This behavior was also found in the analogous InGaAs experiment [14] [Fig. 1(c)]. Let us remark that these theoretical predictions for effective Fourier's law are also in agreement with other previous works [3], where the only way the authors found to describe the observed thermal profile with Fourier's law was to use nonisotropic thermal conductivities for in-plane and out-of-plane directions. However, silicon is an isotropic material and then the required anisotropy of thermal conductivity is unphysical [14]. In contrast, the hydrodynamic model can match the data assuming isotropic heat transport. The apparently anisotropic response of the heat flow in the substrate is a hydrodynamic effect; namely the heat flow in the vertical (heater-substrate) direction

tends to be maintained due to momentum conservation, thus preventing the flow from making sharp turns when exiting the heater. Alternatively, from a macroscopic point of view, the large heat flux gradients in the in-plane direction close to the boundaries produce a large friction which reduces heat flow in this direction as compared to Fourier's predictions.

This friction effect can also be interpreted in terms of heat vorticity as follows. By introducing the vector identity $\nabla^2\mathbf{Q} = \nabla(\nabla\cdot\mathbf{Q}) - \nabla\times(\nabla\times\mathbf{Q})$ into Eq. (2), in a steady situation ($\nabla\cdot\mathbf{Q}=0$) the heat flux reads $\mathbf{Q} = -\ell^2(\nabla\times\omega) - \kappa\boldsymbol{\nabla}T$, where $\omega = \nabla\times\mathbf{Q}$ is the vorticity of the heat flux. It becomes apparent that vorticity makes the heat flux not parallel to the temperature gradient in the general case [see Fig. 1(a)]. It can be seen after a little algebra that, in the in-plane direction, the vorticity term in the later expression opposes the conduction term; this produces an effective reduction of local temperature at the adjacent substrate as compared to Fourier's predictions in agreement with experiments. Note that models assuming cylindrical symmetry [1,2] are, by construction, nonrotational and then cannot grasp this effect; as a result, these authors have to *ad hoc* increase the thermal boundary resistance to come up with this friction effect in order to better fit data.

Finally, in the analogous experiment performed with an InGaAs substrate [14] it was observed that, for heater lines thinner than 1 μm, KCM can reproduce the experimental data by changing the bulk thermal conductivity to a fitted one. For the silicon substrate studied in this paper, this behavior occurs for linewidths smaller than 200 nm, as can be observed in the Supplemental Material [26]. This effect is probably due to the contribution of superdiffusive Lévy flights, which are captured neither by Fourier's law nor by the present hydrodynamic model [14].

The higher collective nature of Si increases its hydrodynamic response as compared to InGaAs, where alloying reduces the collective behavior of phonons. Thus hydrodynamic effects in silicon dominate superdiffusion at smaller length scales than in InGaAs. A model combining both hydrodynamic behavior and Lévy flights contributions is expected to provide the whole picture of semiconductor heat transport at the nanoscale.

B. Thermal decay in multiple Ni heater lines

As a second application, we apply Eq. (2) to describe the decay of an array of heater lines near each other on top of pure silicon [4]. These arrays are nickel heater lines of width L separated periodically by a distance of $4L$ fabricated on a silicon substrate through a thin native oxide layer (less than 2 nm). A laser generates a short heating pulse on the lines and their thermal decay is measured using pump-probe techniques. The authors find a maximum in the effective TBR as L is reduced; that is, as lines become narrower and closer to each other, the effective TBR increases up to a point around 200 nm, below which it decreases. Consequently, for the closest lines, the substrate seems to evacuate energy better than for lines slightly farther apart. This was interpreted that when the nanoscale heat sources are close enough, collective effects among phonons from the different heater lines increase dissipation efficiency.

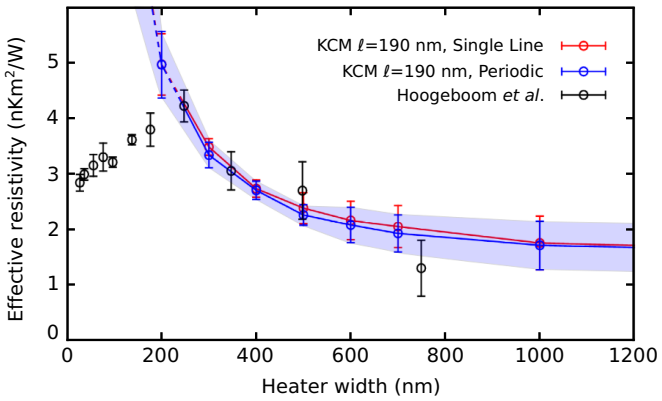

FIG. 2. Effective thermal resistivity as function of the heater width L with periodicity $4L$ on top of silicon. Black dots denote the effective resistivity needed by Fourier law to fit the experimental data (Ref. [1]). Red and blue dots correspond to the effective resistivity needed by Fourier law to reproduce the KCM decay curves for a single line and a periodic array of lines, respectively.

By using finite element methods, Eq. (2) supplies the thermal decay profiles for an isolated heater line and for a periodic array of lines. We use the bulk value $\kappa = 124$ W/mK, and a nonlocal length $\ell = 190$ nm obtained through the expressions described in the Supplemental Material [26]; this value for pure silicon is slightly different from that of the B-doped silicon sample used in the previous experiment. In this case we do not consider any TBR for the thin Ni-native oxide-Si interface, in agreement with the much lower TBR values predicted by the acoustic mismatch model (AMM) and the diffuse mismatch model (DMM) in the case of Ni–native oxide–Si interfaces as compared to those found for Au-oxide-Si [35,36]. In order to compare the KCM predictions with the effective TBR values reported in Ref. [4], we have proceeded as the authors did with experimental data; namely we find the effective TBR required by Fourier's law to match the KCM thermal decay profiles. Interestingly, Fig. 2 shows that the effect of KCM on the temperature distribution is equivalent to the one produced by an effective thermal resistivity in the interface between the heater and the sample, i.e., the TBR [14]. One observes that the hydrodynamic model is able to predict the experimental data for linewidths larger than 200 nm. Then, what is usually considered as a size-dependent TBR can be interpreted just as a hydrodynamic effect resulting from increasing friction as size decreases (since gradients become larger). This is an example of the physical insight provided by the hydrodynamic model. Let us note that it does not only supply a qualitative explanation, but a quantitative one with predictive power: with just the values κ and ℓ, one can predict the TBR value at any system size larger than 200 nm.

Finally, when the heater linewidth decreases below this size the KCM needs a reduced effective resistivity to reproduce observations. Notice that this behavior is similar to the one found in the previous experiment, where KCM could fit experimental data below 200 nm by increasing the bulk thermal conductivity. Again, we believe that explaining the behavior of nanoheater arrays when the linewidth is smaller than 200 nm requires treating both hydrodynamic effects and Lévy

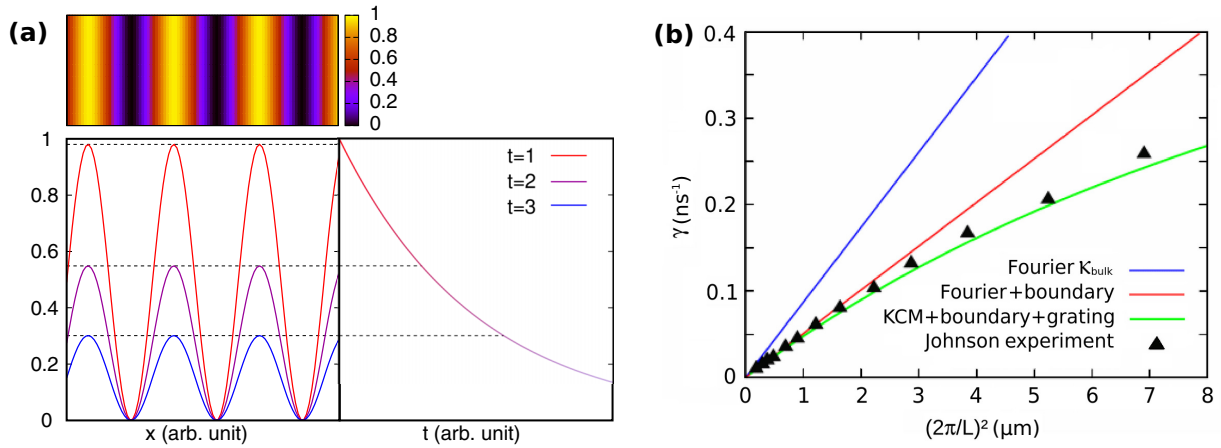

FIG. 3. (a) Typical thermal grating temperature profile and decay curve. (b) Effective decay rate as a function of the square inverse grating length scale: experiments (symbols), Fourier predictions with the bulk heat conductivity (blue line), and hydrodynamic predictions, Eq. (4) (green line) with $\ell = 190$ nm. The red line gives the hydrodynamic prediction for asymptotic long grating periods, i.e., thin films. Film width, $h = 400$ nm.

superdiffusion. Solutions combining both hydrodynamic and fractal diffusion for complex 3D geometries are currently not available.

C. Transient thermal grating on Si

As a third application of the hydrodynamic model, we address the experiments reported in Ref. [2], where an interference grating is used to create a 1D spatial sinusoidal temperature pattern on a silicon membrane and its decay to equilibrium is characterized [Fig. 3(a)]. By combining the energy conservation with Fourier equation using an effective thermal conductivity, the expected decay rate can be obtained:

$$\gamma = \frac{\kappa_{\text{eff}}\zeta^2}{c}, \tag{3}$$

where c is the heat capacity per unit volume, $\zeta = 2\pi/L$ is the inverse length scale, and L is the grating period. Standard Fourier theory predicts a constant thermal conductivity and consequently a quadratic rise of the decay rate as a function of the inverse length scale. Experimental data do not follow this prediction, but show an apparent reduction of the effective conductivity for increasing values of ζ [see Fig. 3(b)].

In this specific configuration, an analytic solution of the one-dimensional version of Eq. (2) can be easily obtained. The spatial derivatives of the heat flux in that equation give a contribution equal to $3\ell^2\zeta^2$, so that the final result for the decay rate is

$$\gamma = \frac{\kappa\zeta^2/c}{1 + 3\ell^2\zeta^2}. \tag{4}$$

However, this 1D result cannot be applied to the experiments described in Ref. [2] with a membrane of small thickness, h, of the order of 400 nm, not much larger than the nonlocal length, ℓ. In this case the transverse coordinate must be taken into account in Eq. (2) and, therefore, the solution deviates from the one-dimensional form. Interestingly, this experimental situation can be solved analytically (see Secs. S3 and S4 in the Supplemental Material [26] for more details). There we show that, for the small values of $\ell\zeta$ that are relevant in the experiment, the effect of the transverse profile is just to substitute the bulk thermal conductivity in Eq. (4) by the effective in-plane conductivity of the membrane, $\kappa(h)$, and the parameter ℓ^2 by an effective value reduced in the same proportion, $\ell^2_{\text{eff}} = \ell^2\kappa_{\text{eff}}/\kappa$. In Fig. 3(b), the experimental results and Fourier's prediction, Eq. (3), using the bulk value of the thermal conductivity are plotted. The KCM prediction given by Eq. (4) with the effective parameters (green line) is also displayed finding agreement with data. Since the substrate here is pure silicon, as in the previous experiment, the same value $\ell = 190$ nm for the nonlocal length is used.

These experimental results are easily interpreted in terms of friction: the two length scales of the system, namely h and L, introduce thermal gradients and thus increase friction. The result is that heat flow decreases and then thermal decay becomes slower. The two length scales play a different role in the thermal decay rate: the membrane width essentially reduces the membrane effective thermal conductivity with respect to the bulk value; this changes the slope in Fig. 3(b) from the blue to the red line. The grating period L provides an additional decrease in the decay rate which becomes apparent when L is of the order of the nonlocal length, ℓ. Then, the straight Fourier dependence changes to a curved dependence.

Finally, effective decay rates similar to the experimental ones have also been obtained using the BTE [2]. The authors attribute the reduced decay rates to a reduction of the thermal conductivity, which is obtained through a phonon suppression function that eliminates phonons from the distribution having mean-free path larger than the grating period. Then, the effect of Eq. (4) is similar to the so-called suppression function [2,5], although in the hydrodynamic framework is the result of a nonlocal term in the heat flux equation.

IV. CONCLUDING REMARKS

A hydrodynamic model has been used to explain the deviations from Fourier's law observed in three recent experiments on nanoscale semiconductors with different geometries. This put in evidence that hydrodynamic heat transport is a pervading

behavior in semiconductors at these scales. The hydrodynamic heat equation can be solved either numerically or, in some simple cases, analytically and we compare its predictions with the complex geometric settings of the experiments analyzed. These include different geometries, and both steady and nonsteady situations.

In the first experiment, we study the full stationary thermal profile on the surface of a bulk B-doped silicon sample submitted to a constantly heated line. This experiment is analogous to the recent experiment on InGaAs [14], where the first evidence of hydrodynamic behavior at temperature has been observed. Here we report the experimental results for a silicon substrate and compare to the hydrodynamic model. In the last two experiments, the hydrodynamic model has been applied to describe the transient behavior in pure silicon samples. We have seen that experiments which have been interpreted by considering a size-dependent thermal boundary resistance (TBR) can be explained as a hydrodynamic effect: as size decreases, gradients become larger, thus generating an increasing friction.

One limitation of the hydrodynamic equation in describing nanoscale experiments is that, below a characteristic length $\sim$300 nm for silicon, it is required to modify the bulk thermal conductivity in order to fully reproduce the experimental data. This deviation from hydrodynamic behavior is interpreted as the result of superdiffusive heat transport, an ingredient that should be added to hydrodynamics to get a complete model of nanoscale heat transport.

Finally, the full solution of the BTE can take into account nonequilibrium behavior of independent phonon modes and the spectral transport of phonons across interfaces by iterative methods [37] or by matrix inversion [16]. Up to now these methods have been successfully applied to uniform thermal gradients. However, its implementation for arbitrary 3D geometries becomes very hard because the thermal gradients appearing in the BTE depend on position and are not known *a priori*. In contrast, the hydrodynamic model can be applied to general 3D geometries via a finite element method, which can be directly combined with current tools used in nanoelectronics modeling and optimization at a manageable computational cost.

ACKNOWLEDGMENTS

We acknowledge the financial support of the Spanish Ministry of Economy and Competitiveness under Grants Consolider nanoTHERM No. CSD2010-00044, No. TEC2015-67462-C2-2-R (MINECO/FEDER), and No. TEC2015-67462-C2-1-R (MINECO/FEDER), and the support of the Department d'Universitats, Recerca i Societat de la Informació (DURSI) of the Generalitat de Catalunya under Grant No. 2017-SGR-1018.

[1] M. E. Siemens, Q. Li, R. Yang, K. K. A. Nelson, E. H. Anderson, M. M. Murnane, and H. C. Kapteyn, Nat. Mater. **9**, 26 (2009).
[2] J. A. Johnson, A. A. Maznev, J. Cuffe, J. K. Eliason, A. J. Minnich, T. Kehoe, C. M. S. Torres, G. Chen, and K. A. Nelson, Phys. Rev. Lett. **110**, 025901 (2013).
[3] R. B. Wilson and D. G. Cahill, Nat. Commun. **5**, 5075 (2014).
[4] K. M. Hoogeboom-Pot, J. N. Hernandez-Charpak, X. Gu, T. D. Frazer, E. H. Anderson, W. Chao, R. W. Falcone, R. Yang, M. M. Murnane, H. C. Kapteyn *et al.*, Proc. Natl. Acad. Sci. USA **112**, 4846 (2015).
[5] Y. Hu, L. Zeng, A. J. Minnich, M. S. Dresselhaus, and G. Chen, Nat. Nanotechnol. **10**, 701 (2015).
[6] B. Vermeersch, J. Carrete, N. Mingo, and A. Shakouri, Phys. Rev. B **91**, 085202 (2015).
[7] B. Vermeersch, A. M. S. Mohammed, G. Pernot, Y. R. Koh, and A. Shakouri, Phys. Rev. B **91**, 085203 (2015).
[8] F. X. Alvarez and D. Jou, Appl. Phys. Lett. **90**, 083109 (2007).
[9] P. Torres, A. Torello, J. Bafaluy, J. Camacho, X. Cartoixà, and F. X. Alvarez, Phys. Rev. B **95**, 165407 (2017).
[10] C. De Tomas, A. Cantarero, A. F. Lopeandia, and F. X. Alvarez, J. Appl. Phys. **115** 164314 (2014).
[11] S. Lee, D. Broido, K. Esfarjani, and G. Chen, Nat. Commun. **6**, 6290 (2015).
[12] A. Cepellotti, G. Fugallo, L. Paulatto, M. Lazzeri, F. Mauri, and N. Marzari, Nat. Commun. **6**, 1 (2015).
[13] A. T. Ramu and J. E. Bowers, Appl. Phys. Lett. **106**, 263102 (2015).
[14] A. Ziabari, P. Torres, B. Vermeersch, Y. Xuan, X. Cartoixà, A. Torelló, J.-H. Bahk, Y. R. Koh, M. Parsa, P. D. Ye, F. X. Alvarez, and A. Shakouri, Nat. Commun. **9**, 255 (2018).
[15] A. Ward, D. A. Broido, D. A. Stewart, and G. Deinzer, Phys. Rev. B **80**, 125203 (2009).
[16] A. Cepellotti and N. Marzari, Phys. Rev. X **6**, 041013 (2016).
[17] L. Lindsay, D. A. Broido, and T. L. Reinecke, Phys. Rev. B **87**, 165201 (2013).
[18] R. A. Guyer and J. A. Krumhansl, Phys. Rev. **148**, 766 (1966).
[19] R. A. Guyer and J. A. Krumhansl, Phys. Rev. **148**, 778 (1966).
[20] D. Jou, J. Casas, and G. Lebon, *Extended Irreversible Thermodynamics*, 4th ed. (Springer, Berlin, 2010).
[21] Y. Guo and M. Wang, Phys. Rep. **595**, 1 (2015).
[22] D. Jou, G. Lebon, and M. Criado-Sancho, Phys. Rev. E **82**, 031128 (2010).
[23] F. X. Alvarez, D. Jou, and A. Sellitto, J. Appl. Phys. **105**, 014317 (2009).
[24] Y. Guo and M. Wang, Phys. Rev. B **97**, 035421 (2018).
[25] P. Torres, F. Alvarez, and X. Cartoixa, Kinetic Collective Model: BTE-based hydrodynamic model for thermal transport, https://physta.github.io/.
[26] See Supplemental Material at http://link.aps.org/supplemental/10.1103/PhysRevMaterials.2.076001 for additional results and simulation details.
[27] A. Sellitto, F. X. Alvarez, and D. Jou, J. Appl. Phys. **107**, 064302 (2010).
[28] A. Sellitto and I. Carlomagno, Proc. R. Soc. A **471**, 20150376 (2015).
[29] D. A. Bandurin, I. Torres, R. Krishna Kumar, M. Ben Shalom, A. Tomadin, A. Principi, G. H. Auton, E. Khestanova, K. S. Novoselov, I. V. Grigorieva *et al.*, Sience **351**, 1055 (2016).
[30] L. Levitov and G. Falkovich, Nat. Phys. **12**, 672 (2016).

[31] C.-Y. Zhu, W. You, and Z.-Y. Li, Sci. Rep. **7**, 9568 (2017).

[32] A. Ziabari, A. Shakouri, Y. Xuan, J.-H. Bahk, Y. Koh, M. Si, P. Ye, and A. Shakouri, in *16th IEEE Intersociety Conference on Thermal and Thermomechanical Phenomena in Electronic Systems (ITHERM.2017.7992490)* (IEEE, 2017), pp. 334–338.

[33] COMSOL-Multiphysics®, *version 5.3*, COMSOL AB, Stockholm, Sweden, www.comsol.com.

[34] X. Xia and K. Mohseni, J. Fluid Mech. **830**, 439 (2017).

[35] R. J. Stevens, A. N. Smith, and P. M. Norris, J. Heat Transf. **127**, 315 (2005).

[36] X. Li, W. Park, Y. P. Chen, and X. Ruan, Proc. ASME **1**, V001T04A006 (2016).

[37] E. K. Lee, L. Yin, Y. Lee, J. W. Lee, S. J. Lee, J. Lee, S. N. Cha, D. Whang, G. S. Hwang, K. Hippalgaonkar *et al.*, Nano Lett. **12**, 2918 (2012); L. Vinet and A. Zhedanov, J. Phys. A: Math. Theor. **44**, 085201 (2011).